Waves in Schwarzschild spacetimes: How strong can imprints of the spacetime curvature be

Janusz Karkowski,[1] Krzysztof Roszkowski,[1] Zdobysław Świerczyński,[2] and Edward Malec[1,3]

[1]*Institute of Physics, Jagiellonian University, 30-059 Cracow, Reymonta 4, Poland*
[2]*Pedagogical University, Cracow, Podchorążych 1, Poland*
[3]*Max-Planck-Institut für Gravitationsphysik, Albert-Einstein-Institut, Am Mühlenberg 1, Golm, Germany*

Emitted radiation can be reprocessed in curved spacetimes, due to the breakdown of the Huyghens principle. A maximization procedure for the energy diffusion allows one to obtain wave packets (gravitational and electromagnetic) that are particularly strongly backscattered. Examples are shown with the backscattered part exceeding by one order the remnants of the initial signals. A robust ringing can be observed, with amplitudes exceeding the leftovers of the main radiation pulse. An analysis of the results obtained allows one to set demands on some parameters in the numerical description of a realistic process of the collapse of two black holes.

I. INTRODUCTION

It has been known essentially since the time of Hadamard [1] that curved spacetimes can affect the propagation of waves. The breakdown of the Huyghens principle [1] (or backscatter, a name adopted by the general relativity community after DeWitt and Brehme [2]) can influence both the energy and the energy flux of a wave signal. Backscatter can leave its imprint on the frequency spectrum and can affect the transmission time. The manifestations of this effect are the so-called tails and, most impressively, the quasinormal modes (QNM's). The literature on backscattering and related phenomena is quite extensive—see [3–23] and numerous references therein.

The QNM's have some features of scattering-type solutions and they have been studied in the context of general relativity for more than three decades [6]. Many of their characteristics are well known for black holes [14], for instance, their (complex) frequency spectrum. An observer located at a fixed space position would find that QNM's oscillate with amplitudes decreasing exponentially in time. The oscillation periods and the damping exponents are the real and the imaginary parts of a frequency, respectively. They depend only on a few global characteristics of black holes—their asymptotic mass, angular momentum, and/or global electric charge. Therefore their identification in an observed wave spectrum would unambiguously identify a black hole (and in fact provide an argument, closest to the direct observation, in favor of the existence of black holes). Extensive reviews are presented in [20] and [21]. Tail terms were studied in the 1970s beginning from Price [8], but interest in them has revived again recently [23].

The spectra of QNM's and the decay exponents of the tails are universal, independent of initial data, but the very existence of QNM's and their amplitudes (as well of the tails) do depend on initial wave conditions. The main aim of this paper is to show the strongest imprints of the spacetime curvature that are present in the form of QNM's in a propagating wave. The implementation of this task requires the separation of the genuine geometric effects from those being built into initial data—notice that even in the Minkowski spacetime one can easily form a QNM-like structure by producing suitable initial data. The simplest possibility is to consider the purely backscattered part of the initial radiation, which is absent in the Minkowski geometry but which always exists in a curved spacetime.

It would be meaningless to try to accomplish our aim by the method of ''trial and error''—by selecting at random various initial wave configurations from the ocean of all possible data. Rather, one should focus on initial data that are ''extremal'' in some sense, which can generate, in the first instance, ''extremal'' asymptotic templates, but also can set bounds on some parameters used in the numerical descriptions. In the present paper, we follow the second strategy, using as a guiding principle the idea of extremizing the so-called diffusion parameter [24] and addressing the following issues. First, we estimate the maximal strength of the backscatter. The corresponding profiles of initial wave packets are found to favor vigorous ringing and/or strong deformation of the initial signals. Second, and in relation to the former point, we obtain information on the process of taking waveforms from specific properties of the backscattered radiation. The order of the rest of this paper is as follows. Section II provides basic information on the wave equations. Section III describes in detail the procedure of maximizing the diffusion parameter and shows exemplary initial data for the wave evolution. Section IV reviews some representative examples of wave templates. In Sec. V we again review those features of the numerical examples that could be useful for the numerical relativists dealing with a full nonlinear description of the collapse of two black holes. Section VI summarizes the main conclusions.

II. BASIC DEFINITIONS AND CONCEPTS

A. Equations

The spacetime geometry is defined by the line element

$$ds^2 = -\eta_R dt^2 + \frac{dR^2}{\eta_R} + R^2 d\Omega^2, \tag{1}$$

where t is a time coordinate, R is the radial areal coordinate,

67 064024-1

$\eta_R = 1 - 2m/R$, and $d\Omega^2 = d\theta^2 + \sin^2\theta d\phi^2$ is the line element on the unit sphere, $0 \leqslant \phi < 2\pi$ and $0 \leqslant \theta \leqslant \pi$. Throughout this paper the Newtonian constant G and the velocity of light c are put equal to 1.

We will study the propagation of polar and axial modes of the quadrupole gravitational waves (GW's) and the dipole electromagnetic waves (EW's) in the Schwarzschild background. The evolution equation has the form

$$(-\partial_t^2 + \partial_{r*}^2)\Psi = V\Psi. \quad (2)$$

Here $r* = R + 2m \ln(R/2m - 1)$ is the tortoise coordinate while the potential term reads for the polar GW

$$V(R) = 6\frac{\eta_R^2}{R^2} + \eta_R \frac{63m^2(1+m/R)}{2R^4(1+3m/2R)^2}; \quad (3)$$

for the axial GW

$$V(R) = 6\frac{\eta_R}{R^2}\left(1 - \frac{m}{R}\right); \quad (4)$$

and for the dipole EW

$$V(R) = 2\frac{\eta_R}{R^2}. \quad (5)$$

The evolution equations corresponding to the first two potentials are called the Zerilli equation [25] and the Regge-Wheeler equation [26], respectively.

B. Conserved energy

Equation (2) possesses a conserved energy

$$E(R,t) = \int_R^\infty \frac{dr}{\eta_r}((\partial_t\Psi)^2 + (\partial_{r*}\Psi)^2 + V\Psi^2); \quad (6)$$

that is, the rate of change of E in a fixed volume equals the total flow through the boundary ([27] and [28]). This agrees (up to a constant factor) with the energy deduced from the stress-energy tensor for the EW. Equation (6) represents a mathematically useful quantity in the case of the gravitational waves, with the density being asymptotically proportional to the density in the quadrupole formula. In either case, the energy conservation becomes important in our forthcoming construction.

Assume that initial data Ψ and $\partial_t\Psi$ vanish inside a sphere having a radius $a > 2m$. From the conservation law one easily finds that the amount of the energy that reaches a distant observer is equal to

$$E_a(\infty) \equiv E(a, t=0) - \delta E_a, \quad (7)$$

where

$$\delta E_a = \int_0^\infty dt((\partial_t\Psi + \partial_{r*}\Psi)^2 + V\Psi^2) \quad (8)$$

([27] and [28]). The integration in Eq. (8) is done along the outgoing null cone that starts from a at $t=0$. In the Minkowski spacetime [set formally $m=0$ in Eq. (2)] all of an initially outgoing radiation would get to infinity; in this case $\delta E_a = 0$, since there is no diffusion through the null cone that expands outward from the initial position $R=a$. It is meaningful to distinguish between the momentarily outgoing and ingoing radiation also in a curved, but asymptotically flat, spacetime. One can give either an operational or an analytic definition. Imagine a directional wave generator that sends all radiation in a fixed direction, when located in an almost flat region. [That makes sense, since it is known from analytic estimates, that the fraction of the backscattered energy must fall off at least as $C \times (2m/a)^2$, where C is of the order of unity [27,28] and [29]. By choosing a sufficiently distant location one can make the diffused energy δE_a arbitrarily small.] This generator, when carefully moved to a strongly curved region, will preserve its property of generating directed radiation, which can be initially purely outgoing (or initially purely ingoing). Alternatively, one can work out an analytic definition. Initial data can always be split into two parts, one "initially outgoing" (defined below; in the Minkowski spacetime that would all get to the infinity) and the other purely ingoing (its form is similar to the former—just change $r* - t$ into $r* + t$ and some signs in the expansion—but it is purely ingoing in the Minkowski spacetime). We will show in Sec. III that the concept of initially outgoing waves is useful in bulding a nontrivial construction, and that fact in itself justifies this notion.

C. Initial data for wave equations

Let us define

$$\bar\Psi(R,t) = \Psi_0(r*-t) + \frac{\Psi_1(r*-t)}{R} + \frac{\Psi_2(r*-t)}{R^2}, \quad (9)$$

where the Ψ_i's $(i=0,1,2)$ satisfy the following relations:

$$\partial_t\Psi_1 = 3\Psi_0, \quad \partial_t\Psi_2 = \Psi_1 - m\partial_t\Psi_1,$$

$$\partial_t\Psi_1 = 3\Psi_0, \quad \partial_t\Psi_2 = \Psi_1 - \frac{m}{2}\partial_t\Psi_1,$$

$$\partial_t\Psi_1 = \Psi_0, \quad \Psi_2 = 0, \quad (10)$$

for the polar GW, axial GW, and dipole EW, respectively. In the Minkowski spacetime the function $\bar\Psi$ exactly solves Eq. (2). We assume that the $\bar\Psi_i(r*,t=0)$'s vanish for $R \leqslant a$. Notice that only one of the three functions (for instance Ψ_0) can be freely chosen.

We will say that the initial data are purely outgoing if on the initial hypersurface $\Psi = \bar\Psi$ and $\partial_t\Psi = \partial_t\bar\Psi$. The full solution of Eq. (2) can now be split into the known part $\bar\Psi$ and an unknown δ,

$$\Psi = \bar\Psi + \delta, \quad (11)$$

with null initial values for δ and $\partial_t \delta$. δ is evolved according to the inhomogeneous wave equation

$$(-\partial_t^2 + \partial_{r*}^2)\delta = V\delta + \tilde{V}, \tag{12}$$

where

$$\tilde{V} = \left(V - 6\frac{\eta_R^2}{R^2}\right)\left(\Psi_0 + \frac{\Psi_1}{R} + \frac{\Psi_2}{R^2}\right) + \frac{2m\,\eta_R}{R^4}\left(-3\Psi_1 + 2\frac{\Psi_2}{R}\right) \tag{13}$$

for polar gravitational modes,

$$\tilde{V} = \frac{10m\,\eta_R}{R^5}\Psi_2 \tag{14}$$

for axial GW's, and

$$\tilde{V} = 6m\,\frac{\eta_R}{R^4}\Psi_1 \tag{15}$$

for the electromagnetic case. The splitting (11) has been crucial in obtaining analytic estimates of the backscatter [27–30] but it appears to be advantageous also from the numerical point of view.

III. EXTREMIZING THE DIFFUSION PARAMETER

A. Diffusion parameter and the variational problem

Let us define the reprocessed radiation (RR) as that reaching a distant observer after the passage of the initial pulse; the delay is caused by multiple backscatterings. RR would be absent in the Minkowski spacetime. (For an example, see in Figs. 8–13 below the parts of waveforms to the right of $x = 0$.) We study hereafter the RR generated by initially outgoing waves, in order to separate the genuine effects of the geometric curvature from those implied by artificial initial data.

The diffusion parameter κ is defined as the ratio of the diffused energy and the initial energy,

$$\kappa = \frac{\delta E_a}{E(a,0)}. \tag{16}$$

Our aim in this section is to provide outgoing initial data that maximize κ. This will be done in a class of data that do vanish for $R \leqslant a$. The intuition behind this is that if κ is large then the fraction of the energy of the reprocessed radiation should also be large. That in turn should translate into effects like vigorous ringing modes or tail terms. We conjecture, that there exists a correlation between κ and (defined in some way) the strength of QNM's.

Expressing things in technical terms: we want to maximize the nonnegative quadratic form δE_a while keeping fixed the positive quadratic form $E(a,0)$. In numerical calculations this task reduces to a multidimensional algebraic eigenvalue problem, as we shall demonstrate. In the first step we choose some large $R_1 \gg a$—the upper end of the initial support—and maximize κ in the future domain of dependence of (a,R_1) with the apex at

$$\left(R_2 \equiv R\left[\frac{r^*(R_1) + r^*(a)}{2}\right], t = \frac{r^*(R_1) - r^*(a)}{2}\right).$$

Obviously the change of R_1 would change κ as well, but it has been established that above some critical value of R_1 the value of κ stabilizes. It has been found by the method of trial and error that the choice $R_1 \approx 150m$ is satisfactory.

B. Discretization of the variational problem

In the second step we determine a functional discrete basis $\{f_i\}$ $(i = 1, \ldots, N)$ on the closed interval $[r^*(a), r^*(R_1)]$. The dimension of that basis was usually 250 (but tests with smaller and bigger dimensions were also done)—a number much smaller than the number of points (8000) in the spatial grid; that facilitated greatly the numerical calculation, without losing accuracy. The best results were obtained for the basis consisting of the first 250 Legendre polynomials with odd indices.

Let the expansion of the function Ψ_0 [the only free function in the initial data set—see the remark following Eq. (10)] be

$$\Psi_0(r^*, t) = \sum_{i=1}^{N} C_i f_i\left(\frac{r^* - t - r^*(a)}{r^*(R_1) - r^*(a)}\right). \tag{17}$$

Then one finds from Eq. (6) that the total initial energy has a positive definite quadratic form:

$$E(a, R_1, t=0) = \int_a^{R_1} \frac{dr}{\eta_r}((\partial_t\Psi)^2 + (\partial_{r*}\Psi)^2 + V\Psi^2)\Big|_{t=0}$$

$$= \sum_{i,j=1}^{N} B_{ij}(a, R_1) C_i C_j, \tag{18}$$

where the matrix B_{ij} is known from numerical calculation.

Each element $\Psi_{0,i} = f_i$ determines some initial values $(\Psi_{f_i})_{t=0}, (\partial_t\Psi_{f_i})_{t=0}$; they give rise to solutions Ψ_{f_i} in the domain of dependence. These solutions are linearly independent [due to the uniqueness of solutions of Eq. (2)]. Therefore the solution generated by the initial data defined by Eq. (17) can be expressed as the linear combination

$$\Psi(r^*, t) = \sum_{i=1}^{N} C_i \Psi_{f_i}. \tag{19}$$

Thus the energy δE_a diffused through the null cone connecting $(a,0)$ with (R_2, t) has the form

$$\delta E(a, R_2) = \sum_{i,j=1}^{N} A_{ij}(a, R_1) C_i C_j. \tag{20}$$

Again the matrix A is obtained numerically.

The task of maximizing the ratio of the two quadratic forms is equivalent to finding eigenvalues in the generalized eigenvalue problem
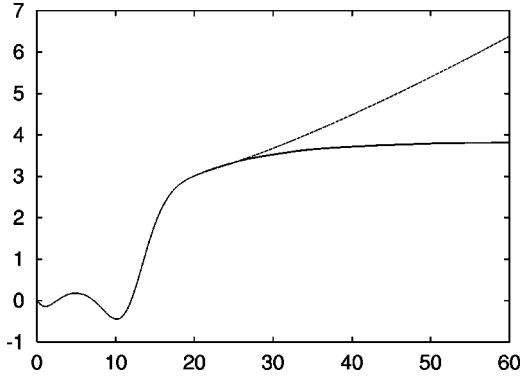
FIG. 1. An eigenvector is matched to an asymptotically constant function (lower branch, solid line). The upper branch (broken line) represents the eigenvector before matching. The x axis shows $r^* - r^*(a)$ and is scaled in units of m.

$$\sum_{j=1}^{N} A_{ij} C_j = \lambda \sum_{j=1}^{N} B_{ij} C_j, \tag{21}$$

where λ is the eigenvalue and (C_i) is the corresponding eigenvector. There are many excellent numerical procedures for solving the generalized problem. We chose one from the fast EISPACK package. This allowed us to find several largest eigenvalues $\lambda^{(k)}$, the eigenvectors $(C_j^{(k)})$, and, from Eq. (17), the corresponding functions $\Psi_0^{(k)}(a, R_1, N)$ for $k = 1, 2 \ldots$. Having $\Psi_0^{(k)}$ one finds initial data using Eqs. (9) and (10).

As a consistency check, in a number of cases the wave packet given by $\Psi_0(a, R_1, N)$ was evolved and the diffusion parameter was found directly from the definition. In the case of disagreement the procedure could be repeated with other values of numerical parameters. A disagreement was never observed for the vectors maximizing κ, but it was found in number of cases with fourth and fifth eigenvectors (by convention, the eigenvectors are ordered according to decreasing eigenvalues, $\lambda_1 > \lambda_2 > \cdots$). The parameters ($N = 250$, $r^*(R_1) \approx r^*(a) + 160m$, the size of the grid) that are reported above seem to be optimal, in the sense that the corresponding integration time was not too long while the accuracy was reasonably good. These values were obtained by performing many series of numerical calculations.

C. Final preparation of extremal initial data

These pre-prepared initial data that are maximizing within the chosen region [in the future dependence zone of data defined on (a, R_1)] undergo a process of extending the initial data beyond R_1. Strictly, we match a function

$$f(r^*) = C_2 + C_1 \exp(-r^*/10) \tag{22}$$

to each eigenvector $\Psi_0^{(k)}(a, R_1, N)$. The matching is differentiable and the gluing point G is selected independently for each eigenvector. The value of G was obtained as follows. Fixing a and R_1, one finds $\Psi_0^{R_1}$ (the upper index is put here in order to stress the local character of the procedure) and
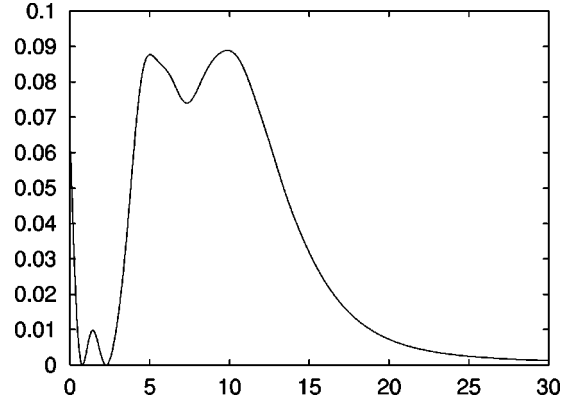

FIG. 2. Axial GW. Initial energy densities for the first eigenvector. Here $a = 2.01$. The x axis shows values of $r^* - r^*(a)$ and is scaled in units of m.

initial values of the locally extremizing solution Ψ^{R_1}. With an increase of R_1, while keeping a fixed, the function $\Psi_0^{R_1}$ changes. In the limit one should in principle obtain the sought-after extremizing solution $\Psi = \lim_{R_1 \to \infty} \Psi^{R_1}$. In numerical practice the integration region must be finite. The dependence of Ψ_0 on R_1 suggests that $\Psi_0^{R_1} \approx$ const outside some region of compact support. The point G is numerically determined as being some point near the transition region. In our case we obtained $r^*(8m) \lesssim r^*(G) \lesssim r^*(25m)$. Therefore the chosen Ψ_0 approaches an asymptotically constant value. Figure 1 shows initial profiles of the the third eigenvector Ψ_0 for $a = 2.001$ (GW, the polar mode).

We would like to point out that this process of matching is to a degree arbitrary, and the eigenvectors obtained can be expected to be close (but not necessarily identical) to the extremizing eigenvectors.

IV. NUMERICAL RESULTS

A. Extremizing initial data and κ versus a

Figures 2 and 3 show the distribution of the initial energy densities of the first and the fifth axial GW modes. As one might expect, the mass center is closer to the horizon in the case of the extremal data, while (not so obviously) the graph of the fifth vector suggests a larger contribution of high frequency radiation.
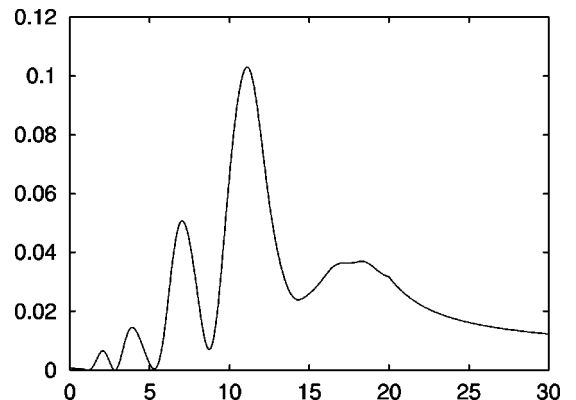

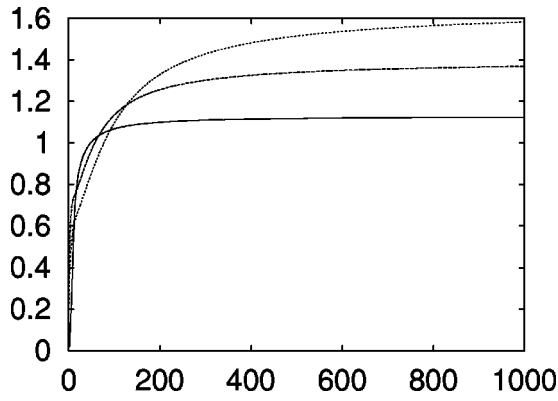FIG. 3. As Fig. 2, but for the fifth eigenvector.

FIG. 4. Polar GW. Initial energy $E(R) \equiv E(a,0) - E(R,0)$ $\times$ (y axis) as a function of $r^* - r^*(a)$ for $a = 2.1m$ (solid line), $a = 3.1m$ (broken line), and $a = 4m$ (dotted line). The scale of the ordinate is arbitrary while the abscissa is in units of m.

Figure 4 demonstrates that the energy support of maximizing initial data increases with the increase of a. The larger a, the larger the distance at which the value of the energy stabilizes. That feature of the maximal initial data is counterintuitive at first glance, since the backscatter is strongest in regions with large values of the potential V (around $R \approx 3m$ or $r^* \approx 0$) and one would expect accumulation of the energy near a if $a \gg 2m$. The reason why it is not so is that the backscatter depends also on the frequency; radiation accumulated at a would be dominated by high frequency waves, which are weakly backscattered.

The main lesson that can be drawn from the foregoing discussion is that the extremizing initial data can occupy a large region that extends far away from the black hole horizon.

A question arises as to whether one can have modes with large κ in the case of waves that are initially well separated from the horizon, i.e., when $a \gg 2m$. As it happens, in order to give an answer one has to combine the numerical approach and an analytic insight. This is because the numerical time is proportional (with some large coefficient) to $(a/2m)^2$
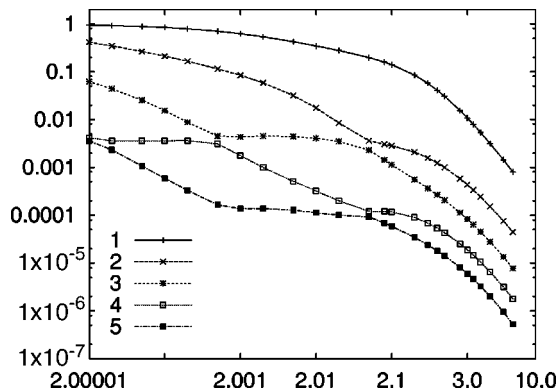

FIG. 5. Eigenvalues κ for the first five eigenvectors for the dipole EW in dependence on a. The points are connected by lines (solid, broken, etc.) in order to make easier the identification of eigenvectors. The x axis shows the position of a and is scaled in units of m.
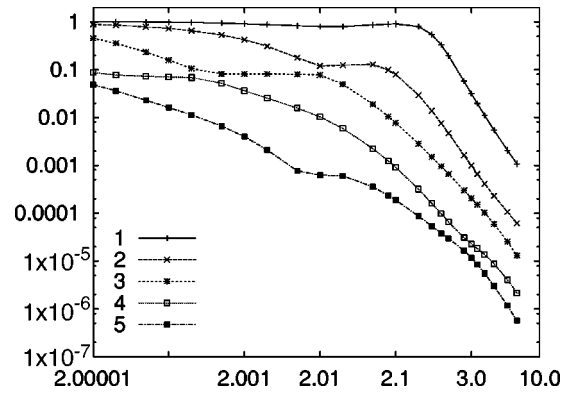

FIG. 6. As Fig. 5 for the axial GW.

and the numerics is feasible only when a is not too big. Fortunately, analytic estimates show that the diffusion parameter quickly decreases with increasing distance, at least as quickly as $(2m/a)^2$, and becomes small at large a [31]. Therefore, if $a \gg 2m$ no modes with large κ can exist, and it suffices to restrict the present analysis to a being relatively small. In this paper the numerics is done for $a \lesssim 6m$.

Figures 5–7 show the dependence of κ on a for the five successive eigenvectors with largest eigenvalues, in each of the considered wave sectors. While at a very close to $2m$ the largest eigenvalue is close to 1 in all three cases, the eigenvalue fifth in the order is smaller than 0.01 for EW's and close to 0.1 for polar GW's, with the axial GW's lying in between. The next observation that should be made is that with an increase of a, the largest eigenvalue changes more slowly than the remaining ones and the falloff of eigenvalues is quickest for EW's and slowest for polar GW's.

B. Stability of templates

Our earlier observation that QNM's can be born and can die [24], when observation points are moved away from the black hole horizon, can be rephrased as a demonstration that *templates can critically depend on the distance of an observer from the horizon*. Below we repeat that study and establish a lower bound on the distance of the observer from the horizon that is needed in order to detect a reliable wave profile.
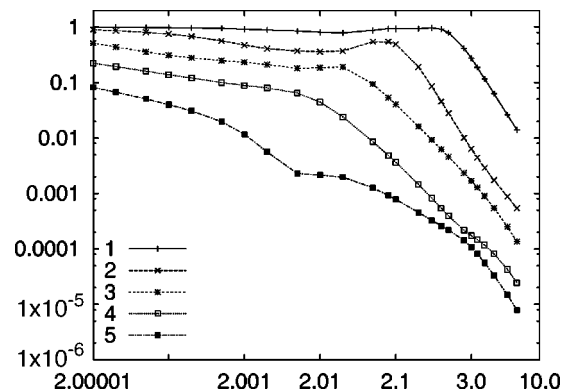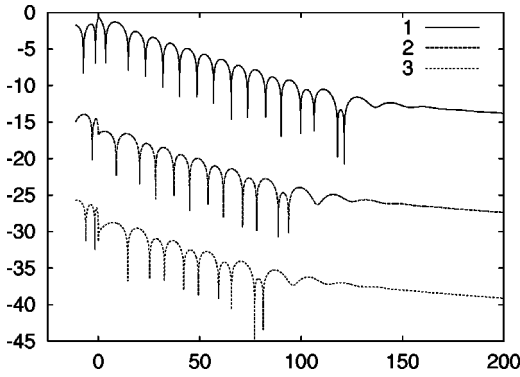

FIG. 7. As Fig. 5 for the polar GW.

FIG. 8. Polar GW, $a=3m$. Waveforms $(\ln|\Psi|)$ generated by the three strongest eigenvectors (no. 1, solid line, no. 2, broken line, and no. 3, dotted line), taken at $R=10m$ (Fig. 8). The abscissa is in units of m. The scale of the ordinate is arbitrary and the amplitudes of each type of eigenvector are properly normalized, for the sake of clarity. The data to the right of $x=0$ correspond to the purely backscattered radiation.

Figure 8 shows that there are many oscillations at $R=10m$, which gradually die when the observation point is moved away to $R=100m$ (Fig. 10 below). One can see that only the first eigenvector produces some distorted oscillations at $R=100m$ while the remaining two fail completely to show any ringing.

Notice that, while the amplitude of the surviving QNM seems to increase moderately, the tail (and pretail) part extends and significantly gains in power. This agrees with the conclusions of [24]. Particularly interesting is the comparison of templates shown in Fig. 9, taken at $R=25m$ [32] and in Fig. 10, determined at $R=100m$. They are clearly different—the ringing phase can be much shorter or even disappear, while the remnants of the initial data (the parts of the diagrams to the left of $x=0$) seen at $R=25m$ are completely different from those detected at $R=100m$. One can conclude that *the process of taking waveforms is unstable under the translation of the observation point*—the templates can strongly depend on the location of the observer.

One can also infer from the preceding information that $25m$ is too close to be the observation point and $100m$ may well be the lower bound for the observer's position. To this point, let us add that in many analyzed examples (not re-
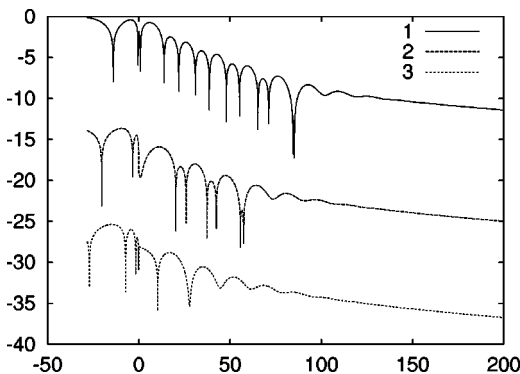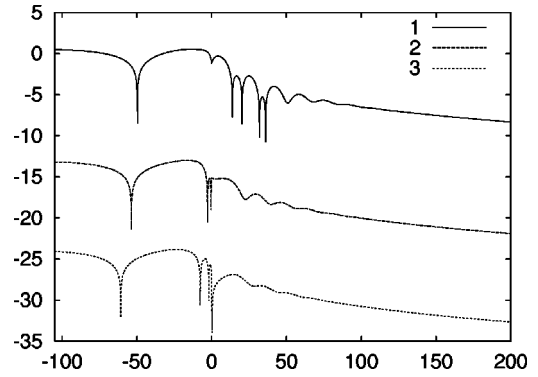

FIG. 10. As Fig. 8 for $R=100m$.

ported here) the waveforms did not change significantly above $R=100m$.

C. Strong ringing modes

One of our aims is to find initial data that give the strongest possible ringing within the reprocessed radiation. The diffusion energy δE_a bounds the energies of QNM's, the tail (and pretail) term, and also the radiation falling into a black hole. While we do not have analytic estimates of the shares of the particular contributing terms in δE_a, it is obvious that configurations with large κ have some room for robust oscillations. For that reason we study waves defined by the extremal initial data.

Figures 11–13 present the radiation corresponding to the EW and GW initial pulses as seen by an "observer" situated at $R=100m$. The $x=0$ point of the abscissa corresponds to the moment of time $t=r^*(100m)-r^*(a)$. This train of data that moves with the speed of light is seen earlier $[t<100m-r^*(a)]$ and it lies to the left of $x=0$. To the right of $x=0$ we have $t>100m-r^*(a)$; in the absence of backscattering there would be no signal at all.

Notice that the amplitudes of the strongest ringing mode are of the order of the largest amplitudes of remnants of the original radiation. This is particularly clearly manifested in the case of the strongest polar GW eigenvector. Observe also a strong deformation of the original signal just before t
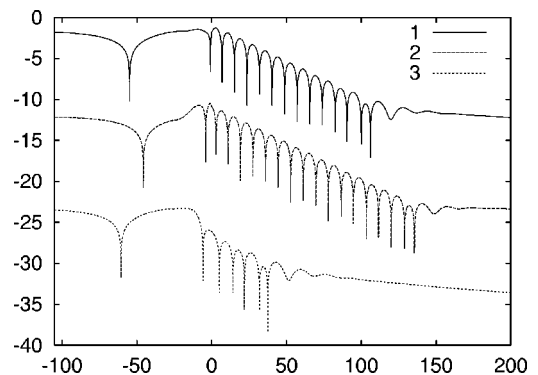

FIG. 11. Templates $(\ln|\Psi|)$ of the axial GW for the three strongest eigenvectors (depicted as in Figs. 8–10). The "observer" is located at $R=100m$ and the parameter $a=2.001$. The part to the right of $x=0$ is the purely backscattered radiation.
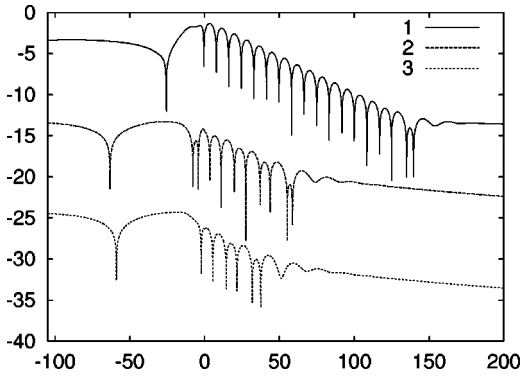

FIG. 9. As Fig. 8 for $R=25m$.

FIG. 12. As Fig. 11 for the polar GW.

FIG. 13. As Fig. 11 for the EW's.

$=r^*(100m)$; initial waveform would be zero at $x=0$, while in Figs. 8–13 one can see a gradual buildup of a backscattered signal. Again, the effect is strongest for the polar GW (Fig. 12, the first eigenvector), when the backscattered part exceeds the remaining signal by a factor of 10. We would also like to direct the attention of the reader to Fig. 10. There the ringing is absent for the second and third eigenvectors, but a very strong pretail term is observed, comparable to the remainder of the main signal.

These examples essentially confirm our conjecture that there exists a correlation between the diffusion factor and some features (strongest QNM and/or the longevity of the ringing phase) of the ringing. (The reservation "essentially" is caused by the fact that the ringing belonging to the second axial mode in Fig. 12 is stronger than that of the first eigenvector; but in this case the diffusion parameters differ only by a factor of 2.) An intuitive explanation with analytic flavor would be the following. There is effectively a $(\partial_t \Psi)^2$ contribution to the observed energy flux, if the observation point is located far away from the horizon (the asymptotic zone, where radiation is dominated by the Ψ_0-type term and $\partial_t \Psi \approx -\partial_{r*} \Psi$). Quasinormal modes oscillate and therefore they give a more significant contribution to the total backscattered energy than, say, tail terms. Hence small κ would be prohibitive for any ringing, while strong κ leaves this possibility open. This reasoning suggests also that the diffused energy might well be the best measure (imperfect, admittedly) of the energy of quasinormal modes generated by moving wave pulses.

It was reported earlier (see, for instance, Sec. IX in [35]) that there exists a (sharp value of) the critical width (suitably defined) of initial data corresponding to strong ringing and that both sub- and super-critical data generate much weaker ringing. While we observe a kind of similar dependence, it is certainly less dramatic and no sharp indicator seems to be appropriate. Admittedly, we deal with a different situation— there is only an (initially) outgoing radiation, while in [35] there are both (initially) ingoing and outgoing components— but that probably is not relevant. More important might be the different shape of the initial data, here determined by the extremization procedure of the preceding section, but in [35] assumed to be Gaussian.
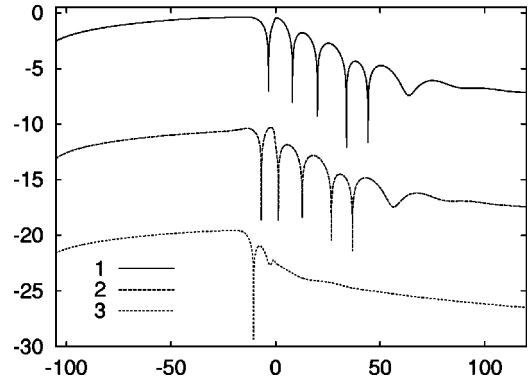
V. LINEAR VERSUS NONLINEAR DESCRIPTIONS OF THE POSTMERGER EVOLUTION

A. How typical are ringing modes?

That is a basic tenet of general relativity, dictated by belief in the cosmic censorship [33] and no-hair conjectures [34], that at some stage after plunge/merger the geometry generated by a pair of black holes can be represented as a single perturbed black hole. The perturbations would be represented by gravitational waves and the final black hole would be either spinning (the Kerr black hole) or nonspinning (the Schwarzschild black hole), the latter in the case of head-on collision. The so-called close limit approximation [36–38] seems to assert that the linear approximation is valid after the formation of a common apparent horizon. Anninos *et al.* [37] give some arguments in favor of this claim that are supported (albeit with some reservations) by their analysis of head-on collisions [39], with initial data of Misner type [40]. Gomez *et al.* [41] provide other supporting arguments in their discussion of fissioning white holes. An interesting new feature of recent work by Husa *et al.* [42], which uses the close approximation, is a weak dependence of the waveforms on the collision velocity of the two black holes.

If this scenario is right then the naive expectation would be that most of the radiation is concentrated in the vicinity of the horizon [43]. (This is in fact observed: see Fig. 10 in [37], which shows that the initial perturbation extends to regions very close to $R=2m$.) One can split these initial data into initially ingoing and outgoing parts, according to the descriptions of Secs. II B and II C. (In the example given in Fig. 10 of [37] the ingoing radiation remains forever inside the potential well [44].) The latter can be expanded in the diagonalizing basis defined in Sec. III and consisting of 250 base vectors, with the parameter a (which in fact specifies this basis—see Sec. III) being very close to $2m$. But if $a \approx 2m$ then Sec. IV A suggests that there appear a number of eigenvectors (from at least 2 for EW's to at least 4–5 in the case of polar GW's) with diffusion parameters being close to 1. The initial data for the linear phase are determined by the preceding nonlinear evolution; if these were purely random, then the chance of having large κ (and strong ringing) would be of the order of 1%. Leaving aside the question of whether the merger phase can be regarded as a random process, the least one can say is that the maximizing initial data of Sec.

III should not be excluded *a priori*. Another argument is that the process of the backscatter is selective—waves longer than QNM's are more strongly backscattered. Since the present gravitational wave detectors are tuned to frequences smaller (even by one order in the case of less massive binaries of black holes [36]) than the QNM's characteristic for the most likely sources of the gravitational radiation, there are reasons to expect that the detected radiation will be strongly backscattered (even if the ringing itself is undetectable).

B. Taking of waveforms: Some parameters

We pointed out in Sec. IV B that in some examples the templates are unstable with respect to a change of the "observation" point. No significant changes in the wave profiles have been observed beyond $100m$, but the wave profiles at $R = 25m$ can be profoundly different from those taken at the former point. This suggests that the determination of templates should be done at $R \gg 25m$ and that $R = 100m$ might be the smallest required distance of the observer. In some cases the duration of the remnants of the original signal and of the backscattered part comparable in strength exceeds $150m$ (see Fig. 12). From this one can infer that the minimal integration time must exceed at least $150m$; it happens to be longer the closer the initial pulse is located to the horizon of a black hole. There is no numerical calculation, in the case of the full nonlinear collisions, to our knowledge, that satisfies both requirements. For instance, in [37], the observations were held at $R = 25m$ through the time interval $100m$.

VI. CONCLUDING REMARKS

The Schwarzschild spacetime is believed to provide a good approximation to the last phase of the collapse of two black holes—the so-called close limit [36–38] is based on this idea—provided that the collision is (almost) head-on. At this stage the spacetime can be regarded as consisting of a single black hole having a mass m and some gravitational radiation that propagates on a Schwarzschlid-type background. The initial data for the linear evolution of the gravitational radiation should be provided by a numerical solution of the preceding phases of the collapse. This task is at present (and presumably for some years to come) unavailable for numerical relativists. In this context the existence of universal imprints of the spacetime curvature like QNM's could be of relevance, but only if their amplitudes are strong enough.

We invent a variational procedure that generates initial data corresponding to strong backscatter. These initial data have some features that might look counterintuitive; they have an extended support and a significant fraction of the wave signal energy comes from a distant region ($R \gg 2m$). They generate strong ringing modes or (if the ringing is absent) robust terms preceding the tail. In many cases the backscattered terms and QNM's are much stronger than the remnants of the original signal; therefore the QNM's waveforms cannot be ruled out as objects of interest for gravitational wave astrophysics.

Finally, it has been shown how from the linear description one can get clues as to the preparation of templates in the numerical analysis of the full nonlinear problem of collapsing (head-on) black holes.

ACKNOWLEDGMENTS

[1] J. Hadamard, *Lectures on Cauchy's Problem in Linear Partial Differential Equations* (Yale University Press, New Haven, CT, 1923).

[2] B. DeWitt and R. W. Brehme, Ann. Phys. (N.Y.) **9**, 220 (1960).

[3] W. Kundt and E. T. Newman, J. Math. Phys. **9**, 2193 (1968).

[4] R. G. McLenaghan, Proc. Cambridge Philos. Soc. **65**, 139 (1969).

[5] W. B. Bonnor and M. A. Rotenberg, Proc. R. Soc. London **A289**, 247 (1967).

[6] C. V. Vishveshwara, Nature (London) **227**, 936 (1970).

[7] W. H. Press, Astrophys. J., Lett. Ed. **170**, L105 (1971).

[8] R. Price, Phys. Rev. D **5**, 2419 (1972).

[9] J. M. Bardeen and W. H. Press, J. Math. Phys. **14**, 7 (1973).

[10] B. Mashhoon, Phys. Rev. D **7**, 2807 (1973).

[11] J. Bicak, Gen. Relativ. Gravit. **3**, 331 (1972); **12**, 195 (1980).

[12] S. Chandrasekhar, *The Mathematical Theory of Black Holes* (Clarendon, Oxford, 1983).

[13] V. Ferrari and B. Mashhoon, Phys. Rev. Lett. **52**, 1361 (1984); Phys. Rev. D **30**, 295 (1984).

[14] E. W. Leaver, Proc. R. Soc. London **A402**, 286 (1986).

[15] N. Andersson, Proc. R. Soc. London **A439**, 47 (1992).

[16] H. G. Nollert and B. Schmidt, Phys. Rev. D **45**, 2617 (1992).

[17] L. Blanchet and G. Schäfer, Class. Quantum Grav. **10**, 2699 (1993).

[18] E. S. C. Ching *et al.*, Phys. Rev. Lett. **74**, 2414 (1995); Phys. Rev. D **52**, 2118 (1995).

[19] E. Malec, N. O'Murchadha, and T. Chmaj, Class. Quantum Grav. **15**, 1653 (1998).

[20] K. D. Kokkotas and B. Schmidt, Living Rev. Relativ. **2**, 2 (1999).

[21] H. P. Nollert, Class. Quantum Grav. **16**, R159 (1999).

[22] K. Roszkowski, Class. Quantum Grav. **18**, 2305 (2001).

[23] J. Stalker, lecture delivered during the Cargese Summer School, 2002.

[24] J. Karkowski, E. Malec, and Z Świerczyński, Acta Phys. Pol. B **34**, 59 (2003).

[25] F. Zerilli, Phys. Rev. Lett. **24**, 737 (1970); Phys. Rev. D **2**, 2141 (1970).

[26] T. Regge and J. A. Wheeler, Phys. Rev. **108**, 1063 (1957).

[27] J. Karkowski, E. Malec, and Z. Świerczyński, Acta Phys. Pol. B **32**, 3593 (2001).

[28] J. Karkowski, E. Malec, and Z. Świerczyński, Class. Quantum Grav. **19**, 953 (2002).

[29] E. Malec and G. Schäfer, Phys. Rev. D **64**, 044012 (2001).

[30] E. Malec, Phys. Rev. D **62**, 084034 (2000).

[31] The estimates are relatively sharp for the EW and axial GW [28] and [27] and exclude any significant backscatter at $a \geqslant 6m$ and $a \geqslant 10m$, respectively. The estimates of [29] for the polar GW require some enhancement, but they are effective for $a \geqslant 20m$.

[32] $R = 25m$ seems to be the canonical choice for the determination of waveforms—see [37].

[33] R. Penrose, Riv. Nuovo Cimento **1**, 252 (1969).

[34] P. Mazur, J. Phys. A **15**, 3173 (1982).

[35] N. Andersson, Phys. Rev. D **51**, 353 (1994).

[36] J. Pullin, Prog. Theor. Phys. Suppl. **136**, 107 (1999).

[37] P. Anninos, R. H. Price, J. Pullin, E. Seidel, and W.-M. Suen, Phys. Rev. D **52**, 4462 (1995).

[38] R. Gleiser, G. Khanna, R. Price, and J. Pullin, New J. Phys. **2**, 3 (2000).

[39] L. Smarr, A. Ćadeź, B. DeWitt, and K. Eppley, Phys. Rev. D **14**, 2443 (1976).

[40] C. Misner, Phys. Rev. **118**, 1110 (1960).

[41] R. Gomez, S. Husa, L. Lehner, and J. Winicour, Phys. Rev. D **66**, 064019 (2002).

[42] S. Husa, Y. Zlochower, R. Gomez, and J. Winicour, Phys. Rev. D **65**, 084034 (2002).

[43] This is plausible and implicitly always assumed to be true by numerical relativists but remains unproven. The main difficulty has its roots in the absence of the notion of a local energy density for free gravitational fields.

[44] The right-hand side of Eq. (2) becomes very small when $r^* \ll -1$ and the ingoing part is not backscattered near the horizon.